# Cellular Chaos: Statistically Self-Similar Structures based on Chaos Game

# **Noah Hill**

J. Mike Walker '66 Department of Mechanical Engineering, Texas A&M University, College Station, TX

# **Mena Maurice**

J. Mike Walker '66 Department of Mechanical Engineering, Texas A&M University, College Station, TX

# **Matt Ebert**

J. Mike Walker '66 Department of Mechanical Engineering, Texas A&M University, College Station, TX \*this auther contributed equally to the first author

# Vinayak Krishnamurthy

J. Mike Walker '66 Department of Mechanical Engineering, Texas A&M University, College Station, TX Department of Computer Science and Engineering (by affiliation), Texas A&M University, College Station, TX Email: vinayak@tamu.edu

We present a novel methodology to generate mechanical structures based on fractal geometry by using the chaos game, which generates self-similar point sets within a polygon. Using the Voronoi decomposition of these points, we are able to generate groups of self-similar structures that can be related back to their chaos game parameters, namely the polygonal domain, fractional distance, and number of samples. Our approach explores the use of forward design of generative structures, which in some cases can be easier to use for designing than inverse generative design techniques. To this end, the central hypothesis of our work is that structures generated using the chaos game can generate families of self-similar structures that, while not identical, exhibit similar mechanical behavior in a statistical sense. We present a systematic study of these self-similar structures through modal analysis and tensile loading and demonstrate a preliminary confirmation of our hypothesis.

# 1 INTRODUCTION

Generative design of engineered structures is now a popular area of research spanning domains including structural mechanics, acoustics, and thermo-fluidics. In a typical generative structural design workflow, the designer defines a spatial domain along with some mechanical conditions and constraints, and the modeling system generates a population of feasible structural alternatives to choose from. A fundamental requirement for a such a workflow is the ability to generate families of structures that possess shared behavioral (e.g. thermal, mechanical, etc.) characteristics making each structure "distinct but feasible". However, the generation of the alternatives, almost always, requires solving an inverse structural problem which is both conceptually and computationally challenging [1, 2, 3].

The objective of this work is to develop and investigate a forward-design methodology for generating families of structures that, while not identical, exhibit similar mechanical behavior in a statistical sense. More importantly, we seek a methodology that offers explicit parameters to control the mechanical behavior of a structural system. To achieve these goals, we introduce an algorithm to generate a new class of structures, namely *self-similar* structures, inspired by fractal geometry. Our methodology is based on the well-known fractal algo-

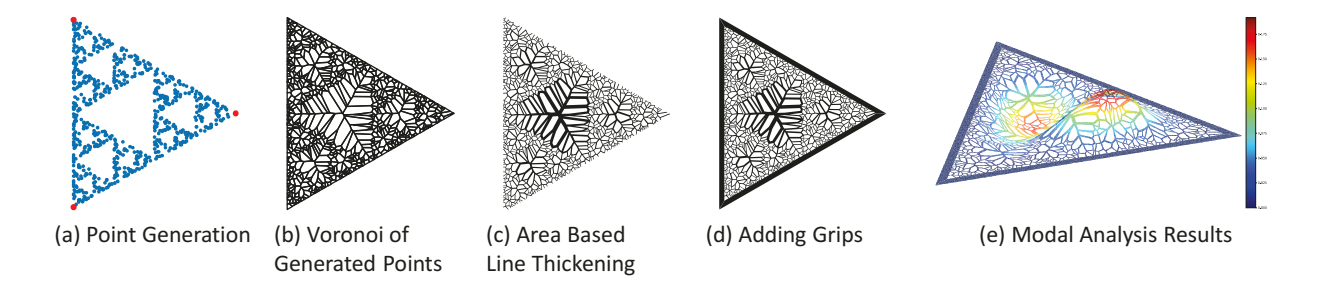


Fig. 1. The method used to generate the points (a), Voronoi Decomposition (b), and the resulting structure(c). In order to test the structure we add grip sections on the exterior of the structure with small gaps between adjacent grips (d). To evaluate the structures we utilized modal analysis (e). The parameters used for generation are n=3,  $\lambda=0.5$ , and t=750.

rithm known as the chaos game, which is a simple and powerful method to generate fractal geometry. Using point-sets generated from the chaos game, our methodology utilizes the well-known Voronoi tessellation to generate self-similar structures with statistically shared mechanical behavior (Figure 1).

# 1.1 Rationale & Background

Fractals offer a unique property that helps generate similar structures since fractals can be defined as consisting of smaller parts similar to themselves, commonly called recursive self-similarity [4]. Self-similarity is an important property of natural structures (e.g. trees, nacre structures, etc.) and is particularly useful in structural design problems [5, 6]. However, much of the literature primarily uses L-systems and grammar-based algorithms [7, 5]. The common approach of investigation in these approaches is to determine the right parameters for the algorithm to generate the optimal structure for a given application rather than explore methods to generate an entire design space of potentially feasible designs. As a result, very little is explored or understood regarding stochastic similarity in mechanical or other physical properties of structures generated using existing fractal-based structural design.

In contrast to prior works, our objective is to embody the idea of generating populations of feasible alternatives rather than generating one optimal solution to a structural problem. In order to achieve this objective, we identify the chaos game as a potent direction for algorithmic investigation of self-similar structure generation. Chaos game is a well-known iterative process that can be used to create fractal geometry in the form of point-sets through repetitive and randomized generation of points using a polygonal domain [8, 9]. Chaos game has been used in the biomedical field [10, 11], plant modeling [12], and computer graphics [4].

In order to understand why chaos game is an interesting direction, let us consider a simple example — the Sierpinski gasket. A typical way to generate the Sierpinski gasket is through iterative subdivision using Lsystems and turtle graphics [13]. However, the Sierpinski triangle can also be generated by using the chaos game by starting with a triangle and generating a series of points based on randomized linear interpolation with the vertices of the triangle (Figure 3). What is critical to note here is that while the L-systems approach gives the exact geometry of the gasket for each iteration, the chaos game only does so in the limiting case (i.e. when the number of iterations tend to infinity). This has two implications. First, the number of iterations in the chaos game controls the level of subdivisions for the gasket. Second. even for the same number of finite iterations, one gets a completely different point-set because of randomization. In conjunction, both these implications mean that for a given polygon (a triangle in this case), an entire family of geometrically similar point distributions (and therefore structures) can be generated by using merely a few parameters (the number of iterations and the interpolation parameter). The question is whether this geometric similarity carries forward into mechanical behavior.

# 1.2 Technical Approach

Chaos game is an iterative method that generates self-similar point-sets in the limiting case within a polygonal domain. By computing Voronoi tessellations on these point-sets, our method generates mechanical structures that adopt the self-similarity of the point-sets resulting in the fractal distribution of local stiffness.

Our work aims to generate families of non-identical structures with similar mechanical behavior, which are generated in the same manner. In this way, our process is a generative method to create structures. Furthermore, each family is uniquely identifiable from the parameters of the chaos game, namely, the polygonal domain, point interpolation distance, and the number of samples. We present a systematic study of these self-similar structures through modal analysis and demonstrate a preliminary confirmation of our hypothesis.

# 2 RELATED WORK

Our work spans multiple overlapping fields of research in structural design each of which is quite extensive. Here, we discuss works that are either methodologically or contextually relevant to our work.

### 2.1 Unit-cell Structural Design

Structural design has a rich history with several algorithms that seek to develop structural systems with specific physical properties. For example, work by Chu et al. [14] considers the design of cellular structures especially for additive manufacturing. Similarly, we see several works that focus on lattice structures for creating auxetic (negative Poisson's ratio) structures [15, 16, 17]. What is common in these approaches is that they are based on arrangements of some or the other form of a unit cell (often symmetric) and the arrangements are constrained according to some underlying grid-structure. The idea is that one can tune macro- and meso-scale properties by varying a few parameters pertaining to the unit cell geometry [18]. However, the design of the unit-cell, in itself, is not a trivial task. In fact, it is either ad hoc and based on trialand-error or requires significant expertise and intuition.

# 2.2 Topology Optimization

Another widely practiced research direction in this regard is that of topology optimization, wherein the typical goal is to optimize (maximize or minimize) a specific criterion specified by the designer [19, 20]. In these cases, the designer explicitly defines the mechanical loads, constraints, and boundary conditions, and a computer generates a single structure that meets the criteria with the set conditions. In these cases, only a single *optimal* design is generated, and if the designer needs a different structure, the design problem must be redefined. There are also works is based on using topology optimization combined with generative design based on L-Systems for the creation of graph-based structures [21, 22].

# 2.3 Learning-based Structural Design

Many recent works consider the inverse design approach using machine learning methods to generate 2D structures with tunable properties [23]. Recently, we

see topology optimization approaches in conjunction with deep learning methods such as convolutional neural networks (CNN) [24] to generate multi-scale structures spanning micro- and macro-scales. Genetic algorithms have also been used to create optimal designs using a Pareto frontier and multiple objectives [25]. There has also been uses of machine learning algorithms in order to optimize biologically inspired patterns [26].

#### 2.4 Voronoi-based Cellular Structures

One method to create a large number of patterns revolves around using Voronoi decomposition of points in order to obtain cellular structures. One area that has used this is the design of 2D infill structures for 3D printing[27]. In a similar manner 3D Voronoi decomposition can be used to create 3D printed structures with anisotropic behavior which can be helpful in certain application with uneven or varied loading conditions present [28]. Another way that Voronoi decomposition has been used is to generate foam structures which has application in many different areas such as topological interlocking and energy absorption [29]. One interesting application is in 2.5D tile generation wherein different 2D Voronoi layers are stacked on top of one another to create a 3D structure from 2D Voronoi decomposition [30]. Voronoi decomposition has also been used to create metamaterial structures which be very beneficial since they do not rely on the design of a single unit cell but rather the design of the Voronoi sites [31, 32].

# 2.5 Fractal-based Structural Design

The chaos game has been used to explore the mechanical properties of fractals when applied as lattice structures [33, 34, 35]. This is done by geometrically defining a structure through lengths, widths, and thicknesses, which can be modified to change mechanical behavior. Similar works have done experiments on hierarchical structures, which can be defined by self similarly at multiple dimensions [36, 37, 38].

# 2.6 Our Work

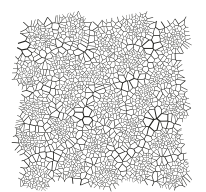
Our work leverages the strength of fractal-based approaches (especially the chaos game) for inducing controllable stochastic variability along with Voronoi-based approaches for elegant topology generation for structure generation. This powerful combination provides advantages over prior approaches by introducing an intuitive way for both parametric control as well as structure generation. In effect, this provides us a means for direct creation of entire families of structures that behave in some



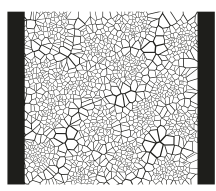
(a) Wallpaper Symmetry Generation



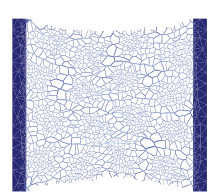
(b) Generate Chaos points on each polygon



(c) Generate Voronoi Structure



(d) Create Tensile Sample with Grips



(e) Test Structure in Tension

Fig. 2. The method used to generate structures for tensile testing through the use of periodic wallpaper pattern (a) where each polygon is used to generate chaos points(b). The chaos points are used with Voronoi and to create a structure and grips (c,d). This structure can be used to simulate under tensile loading (e).

Succession of Points	10 Points	100 Points	500 Points	
	1 1 3 4 4 4 4 4 4 4 4 4 4 4 4 4 4 4 4 4			

Fig. 3. Creation of Points Using Chaos Game Algorithm where n=3 and  $\lambda=0.5\,$ 

stochastically similar manner without the need for inverse design.

### 3 CONCEPTUAL PRELIMINARIES

The chaos theory has been used to define a method for creating fractals, commonly called the chaos game [39, 40, 41]. The chaos game is an algorithm used to generate a fractal that is described as an Iterative Function System, which is a set of pairs of linear mappings [39, 40]. Many different fractals can be generated using different parameters one of the most common is the Sierpiński triangle [41, 42]. The same process can be used to create the Sierpiński pentagon as well as 3D shapes such as the Menger sponge and Sierpiński pyramid.

# 3.1 Chaos Game

The chaos game's process to generate fractals is defined as follows (Figure 3). Consider a polygon,  $P_n$ , where n is the number of vertices of the polygon. The polygon's vertices are defined by the set of points  $\{p_1, p_2, ..., p_n\}$ . For each vertex, the value of  $p_i = (\cos\theta_i, \sin\theta_i)$ , where  $\theta_i = \frac{2\pi * i}{n}$ . This creates a regular polygon with n number of vertices. Consider a randomly placed point  $q_0 \in \mathbb{R}^2$ . We define a function R(n): [1,n] => i which provides the random integer, i, from 1 to i. The i-th vertex of i-i0, which is i1,

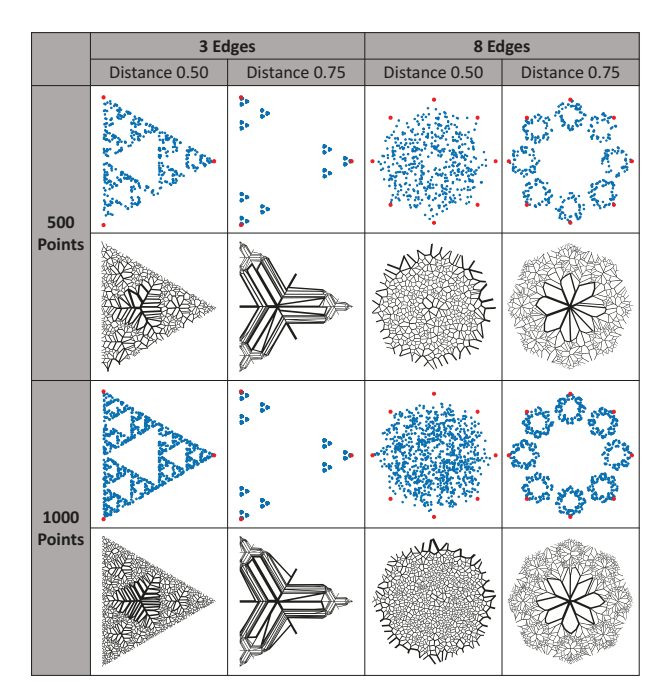


Fig. 4. Structures generated using different combinations of parameter sets are shown here. The effects of varying number of vertices (n), number of points (t), and fractional distance moved along the line  $(\lambda)$  on the generated points and structures are displayed.

is chosen using this function. Using this randomly selected vertex,  $p_i$ , and the randomly chosen point,  $q_0$ , a new point can be defined using the following equation  $q_1 := q_0 + \lambda(p_i - q_0)$ , where  $\lambda$  is the fractional distance moved along the line connecting the vertex,  $p_i$ , and the initial point,  $q_0$ , and defined as  $\lambda \in [0,1]$ . This process can now be repeated for the new point,  $q_1$ . Using t to represent the current iteration, the following equation for

finding the next point can be defined.

$$q_{t+1} \leftarrow q_t + \lambda (p_{R(n)} - q_t) \tag{1}$$

#### 3.2 Parameters

This gives three parameters for the chaos game: n,  $\lambda$ , and t. The first parameter n is the number of vertices of the polygon. These vertices are often called attractors in previous literature [39]. Using different polygons changes the options available for  $p_i$  and the possible values of  $q_t$  (Figure 4). The second parameter is  $\lambda$ , or the fractional distance moved along the line connecting  $p_i$ and  $q_t$ . The fractional distance moved along the line,  $\lambda$  is confined to be between 0 and 1. When  $\lambda = 0$ ,  $q_{t+1} = q_t$ , conversely when  $\lambda = 1$ ,  $q_{t+1} = p_i$ . This means that if  $\lambda$  is closer to 1, the points will be clustered towards the vertices of the polygon, while if  $\lambda = 0$ , the points will be more clustered in the center of the polygon (Figure 4). The third parameter is T, the number of iterations being run. The current iteration, t, is defined as  $t \in [t_0, T]$ , where  $t_0 > 0$  and T is the number of iterations. Since the initial point  $q_0$  is not guaranteed to be within the polygon, several initial iterations are done before the number of iterations starts counting( $t_0$ ), and all points generated before  $t_0$  are ignored. Changing the number of points generated changes how densely the polygon is filled, which changes the structure being generated and how that structure may react when tested (Figure 4).

### 3.3 Generating Points

By defining all three parameters, a set of points can be generated using the defined algorithm (Figure 3). The set of points is defined as  $S := \{q_t\}$ , where all  $q_t$  are inside the main polygon. The set of points will be called the *chaos sites*. These *chaos sites* can be used to create the structures being studied (Figure 1a).

Since the number of points being generated is finite, getting different sets of points with the same parameters is likely since the starting random point differs each time. Additionally, successive iterations of R(n) return different chosen points each time, even if the initial point is the same. It is for this reason that this process is generative since, for the same set of parameters, there will be a different (but similar) set of points generated (Figure 5). Different sets of parameters will also result in very different sets of points (Figure 4). For example, five runs with the polygon being a triangle, fractional distance moved along the line being 0.5, and the number of points being 750 will produce five triangles that have a statistically similar clustering of points, but the structure will not be the same across all five runs (Figure 5).

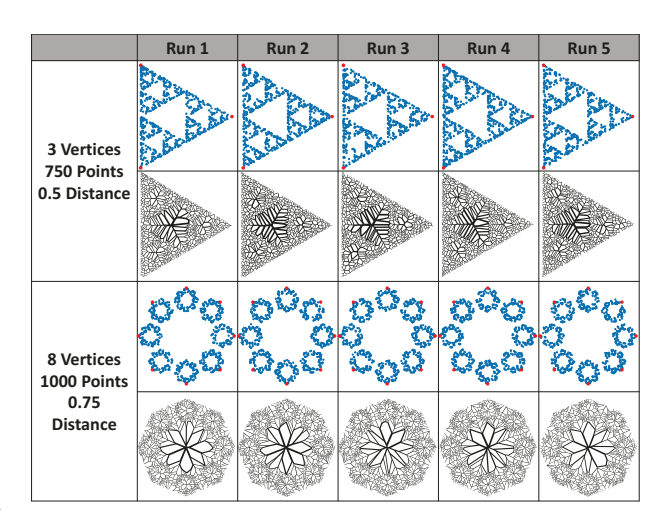


Fig. 5. Five different runs for the same set of parameters produce similar, but not identical points and Voronoi decomposition. This process demonstrates how the method is generative. Two different sets of parameters are shown here.

The polygon used for the chaos game does not have to be a regular polygon like  $P_n$ . Wallpaper symmetries can be used to create a pattern of identical polygons that can be used as the input polygon for the chaos game. Wallpaper symmetries create a set of points by rotating and translating a starting point throughout a domain. Voronoi decomposition can be used on these starting points to create the set of polygons (Figure 2a). A set of chaos sites, S, can now be generated for this polygon. Furthermore, it is also possible to create  $S^*$ , which is defined as the union of multiple S (Figure 2b), in doing so  $S^*$  is generative in the same way since it is the combination of multiple generative sets.  $S^*$  is also a set of chaos sites and can be treated in a similar manner to S during structure creation.

# 4 STRUCTURE GENERATION METHODOL-OGY

The *chaos sites*, S or  $S^*$ , generated using the Chaos Game algorithm can be used to create a structure. The methodology used to generate this structure has two main components: (1) computing a Voronoi tessellation of S or  $S^*$ , (2) thickening the edges of the Voronoi tessellation.

# 4.1 Voronoi Decomposition

To create our structures, a Voronoi tessellation is calculated for the *chaos sites*, S or  $S^*$ , creating a set of cells for the structure. Note that the distribution of points in S is an approximation of some fractal geometry. As a result,

the tessellation of this set results in a partition wherein the cell areas are distributed in a manner inversely proportional to the point density thereby giving the structural a fractal-like property, meaning cell areas are small where there is a high density of points. For modal testing, the unbounded cells resulting from Voronoi tessellation are trimmed according to the polygonal domain boundary (Figure 1b). For tensile testing, the unbounded cells resulting from Voronoi tessellation are trimmed according to the edges of the wallpaper symmetry (Figure 2c).

# 4.2 Edge Thickening

Given a Voronoi tessellation of the polygonal domain, our next step is to thicken the edges in the tessellation. As such, this can simply be achieved by creating offset polygons for each Voronoi cell in the tessellation. However, an important consideration here is that the fractal-like distribution of the chaos sites results in a high variation in the areas of the Voronoi cells. Therefore, we employ an adaptive strategy wherein, we determine the offset for each cell based on the measure of the cell areas normalized with respect to largest and smallest cells in the tessellation (Figure 1c). Specifically, we begin by computing the maximum and minimum cells areas  $(A_{max}$  and  $A_{min}$  respectively. For a given Voronoi cell with an area A, we then compute the *normalized area*,  $\hat{A}$ , as follows (Equation 2):

$$\hat{A} = \frac{A - A_{min}}{A_{max} - A_{min}} \tag{2}$$

Consider an edge e shared by two Voronoi cells  $f_j$  and  $f_j$ . Then, the thickness of the edge is given by  $\tau_e = \omega_1 + \omega_2$ , where  $\omega_i$  and  $\omega_j$  is the offset applied to  $f_i$  and  $f_j$ . Note that for a non-adaptive thickening, this would simply amount to  $\tau_e = 2\omega$  where  $\omega_1 = \omega_2 = \omega$  is a constant offset. However, in our adaptive case, the idea is to compute the offset based on the normalized areas. For this, we define  $\omega_{max}$  and  $\omega_{min}$  as the maximum and minimum possible polygon offsets respectively. For a cell  $f_i$  with normalized area  $\hat{A}_i$ , the offset  $\omega_i$  is calculated by linearly interpolating between the offset limits as (Equation 3):

$$\omega_i = \hat{A}_i(\omega_{max} - \omega_{min}) + \omega_{min} \tag{3}$$

Therefore, the thickness of an edge shared by two Voronoi cells  $f_j$  and  $f_j$  with normalized areas  $\hat{A}_i$  and  $\hat{A}_j$ , the thickness  $\tau_e = (\hat{A}_i + \hat{A}_j)(\omega_{max} - \omega_{min}) + 2\omega_{min}$ .

### 4.3 Grip Generation

In our work, we specifically aim to investigate our shape generation methodology in terms of comparing structures based on their natural frequencies and under tensile loading. In order to do so, we implemented a grip generation step in our computational framework in order to apply fixed or forced displacements during simulation. This is primarily done to ensure the application of appropriate boundary conditions for our analysis. Having said this, this is not a fundamentally necessary step toward the generation of the actual self-similar structure and we have added it for completeness.

In the case of modal testing, we first generate an outward offset for the polygonal domain. This results in a region between the original and the offset polygon. We then split this region into n pieces (where n is the number of sides of the domain) simply by connecting each pair of corresponding vertices in the two polygons. This results in n distinct grips rather than a single body (Figure 1d). For tensile testing, a square is used to define the domain for the structure. Then, we take this square domain and add solid regions to the right and left sides with small thickness so as to not influence the mechanical behavior of the part (Figure 2 d). After the grips have been added, the sample is extruded and triangulated to make it a 3D structure.

### 5 EXPERIMENTAL DESIGN

The central claim behind our method is that the geometric similarities induced by each family of parameters of the chaos game reflects in several mechanical properties. In order to investigate this claim, we conducted a series of numerical experiments wherein we used modal analysis and tensile loading as the mechanical properties to measure. For modal analysis, the idea was to perform comparative statistical analyses of natural frequencies of structures across different selective parameter families (polygonal domain — n, number of iterations — T, fractional distance —  $\lambda$ ). For tensile loading, our goal was to compare stress and deformation behavior across structures generated with multiple different wallpaper symmetries as well as across the chaos parameters. Below, we provided details regarding the design of our experiments.

#### 5.1 Modal Analysis

We chose modal analysis as our first context for two reasons, First, it gives us a concrete physical context (vibrations of a dynamical system) which we can easily quantify in terms of natural frequencies. Second, the modes of a structural system are fundamentally con-

	Parameter Set 1	Parameter Set 2	Parameter Set 3
Points		2 4 4 4 4 4 4 4 4 4 4 4 4 4 4 4 4 4 4 4	
Generated Structure			
Frequency 1			
Frequency 2			
Frequency 3			
Frequency 4			
Scale		0,0000	000 000 000 000 000 000

Fig. 6. Different parameters for shape generation are shown here. The deformation of the first 4 modes is also shown with the scale bar showing the total deformation in meters. The grips shown in the generated structure are disconnected by a small margin.

nected to the geometry and topology of the system. Consequently, this would allow us to make objective comparisons of the mechanical behavior of each structure by examining the natural frequencies and mode shapes of each geometry [43, 44]. Based on these reasons, modal analysis is an ideal candidate for a preliminary exploration of how statistical shape similarities can carry over to mechanical properties.

We implemented our experiments using ANSYS using APDL. Each grip's nodes are fixed which prevents the grips from moving, allowing only the inside structure to be examined with the modal analysis. Once the grips are fixed, the modal analysis is performed, and the results can be analyzed.

# 5.2 Tensile Loading

In order to test the mechanical response under loading, we use tensile testing to evaluate if the proposed method could be a viable generative design technique for 3D printing infills. In order to test this, we first start with

a periodic pattern generated using wallpaper symmetries, the polygons of the resulting periodic pattern can then be input to the chaos games to create S, and all chaos sites can be combined together to create  $S^*$ .  $S^*$  is used along with Voronoi to create a structure. In this manner, the number of vertices used in the chaos game is fixed by the chosen wallpaper symmetry. Note that all the chaos sites S that comprise  $S^*$  use the same parameters, which makes each set S distinct but generated with the same parameters.

To perform these experiments, we used ANSYS APDL, where the structure was assumed to be a 2D planar structure with thickness. The grip on one side is then defined to be fixed, and a forced displacement is applied to the grip on the other end. After running the simulation, all nodes' Von-Mises stress and deformation values are exported and stored for analysis.

# 5.3 Hypothesis

We predict that using the same parameters, the generated structures will not have statistically different mechanical properties over multiple iterations. This hypothesis aims to test if the parameter space defined by the chaos game and using our generation methodology results in structures that belong to the same family which could all be *feasible* design solutions. Ultimately this would show that our methodology is a generative process for creating structures.

If the previous statement holds true, we expect that as we change  $\lambda$  then there should be a linear relationship in the frequency magnitude. This relationship can be expected because  $\lambda$  is the distance moved along a line connected the randomly selected polygon point and the previous point. For this reason we expect a linear relationship between  $\lambda$  and the magnitude of the frequency.

# 5.3.1 Modal Analysis

To test the hypothesis that structures generated with the same set of parameters will have statistically similar results, the same set of parameters was simulated 100 iterations. The parameters n,  $\lambda$ , and t were set to 3 vertices, 0.5 fractional distance moved along the line, and 750 points, respectively. The first ten natural frequencies were found for each of the 100 runs in order for comparison. For each shape generated, we recorded 10 natural frequencies along with the deformation of the shape.

To test the hypothesis that  $\lambda$  and the resulting frequencies were related, a second experimental setup was devised where the number of points was set to 750 and the value of  $\lambda$  would be the following: 0.1, 0.2, 0.3, 0.4, 0.5, 0.6, 0.7, 0.8, and 0.9. For each polygon, we recorded

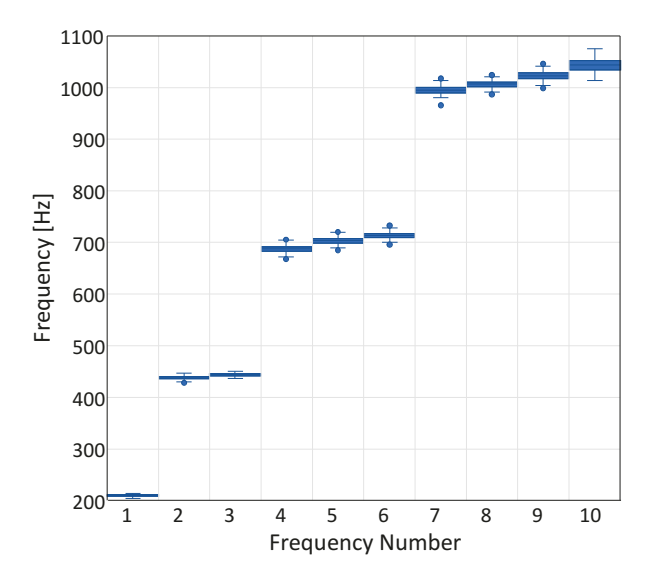


Fig. 7. First 10 Frequencies for the same set of parameters (  $n=3,\,\lambda=0.5$  , and t=750 ) after 100 runs.

5 natural frequencies along with the deformation of the shape for 25 iterations. Additionally the values of n were chosen to be 3, 5, 6, and 8.

#### 5.3.2 Tensile Testing Analysis

With tensile loading, there are many more parameters to measure as opposed to modal analysis, since we impose a displacement into the structure we chose to measure the stress characteristics of the part, specifically the Von-Mises stress distribution, which is a measure of equivalent stress. Since the maximum stress is sensitive to sharp corners, we compare the average stress on the nodes for each structure. With tensile loading of parts, we predict that parts generated with the same parameters will exhibit statistically similar behavior when comparing the average stress. We further posit that the average stress values will be dependant on the wallpaper symmetry (which controls the shape and the variable t), meaning that for different wallpaper symmetries the values of average stress may be very different. The wallpaper symmetries chosen are p2, p3, p4, and p6, which only require rotation of a single starting point and copying (Figure 11.

For each test the porosity was also calculated so as to be compared if necessary and was calculated as the ratio of empty volume to total volume and is represented as a decimal.

#### 6 RESULTS

# 6.1 Modal Testing

The aim of the first test was to determine if structures with the same set of parameters have statistically similar results, in this case, natural frequencies. One hundred iterations were run for a single set of parameters, and the first ten natural frequencies were compared. A one-way ANOVA shows that the null hypothesis is rejected. In other words, there is a significant difference in the population means of the data. This, in turn, supports our central hypothesis that geometric similarities induced by identical parameters also exhibit similar mechanical properties. This is further reinforced by the low standard deviations for each given population (Table 1). An interesting observation is that the standard deviations generally increase as the frequency increases, which can be seen as the standard deviation of frequency 1 is 2.04Hz, and for frequency 10 it is 13.06Hz. As modal frequency increases, the magnitude of the frequencies begin to pair off with one another, with frequency 1 being the exception as it is the only category dissimilar to the other frequencies (Figure 7). We can observe this pairing-off effect in frequencies 2 and 3, which have similar results at near a frequency of 440Hz, and frequencies 4, 5, and 6, which also share similar results near a frequency of 700Hz. Frequencies 7, 8, 9, and 10 also pair together at a value around 1000Hz. An interesting observation is that at higher frequency numbers, the number of frequencies in a pair increases with the first pairing only containing two modes, the second has three, and the third pairing having four pairs. Since many of these frequencies pair together, we used a twosample t-test in order to verify that these frequencies are from two independent populations and not samples from a single population. In each case, the p-value for comparison was < 0.005 showing that it is likely that the pairing originates from two separate populations. Similarly to the pairing behavior of the frequencies, it can be observed that the standard deviations of the different frequency groups pair together, with the first pairing having a standard near 3.4Hz and the second pairing having a standard deviation near 7Hz.

For experiment 2, we tested if the fractional distance moved along the line,  $\lambda$ , has a linear relationship with the frequency. For each of the different polygons tested, we conducted a two-way ANOVA, which showed that the null hypothesis was rejected in each case, meaning that there are significant differences in mean values for  $\lambda$  and frequency number. Additionally, the tests showed that there is an interaction between the two factors. Some general results were found for all the polygons tested. There appears to be a distance at which each frequency value peaks for each polygon (Figure 8). For example, in the

Frequency Number	1	2	3	4	5	6	7	8	9	10
Mean (Hz)	209.5	438.0	443.9	687.3	703.3	713.2	994.5	1006.7	1022.7	1043.7
Standard Deviation $(Hz)$	2.04	3.61	3.22	7.63	7.05	6.68	8.69	7.30	8.43	13.06

Table 1. After 100 runs with the same input parameters, the average and standard deviation are shown.

triangle (n=3), the frequency values peak at  $\lambda=0.4$ . Also, the lowest frequency value for the structures tested tends to occur at  $\lambda=0.9$  (Figure 8). Further, frequencies 1-3 change less as  $\lambda$  increases from one value to the next, while frequencies 4-5 change more as  $\lambda$  increases.

# 6.1.1 Triangle

For the triangle structures (n = 3), the frequency magnitudes tend to form pairs at many values of  $\lambda$  (Figure 8). This can be seen as frequency 1 is often dissimilar to the other values, and frequencies 2 and 3 are often close in magnitude. In a similar manner, frequencies 4 and 5 tend to pair together. For the triangle structures, the pairings stay consistent up to  $\lambda = 0.6$ ; afterward, the pairings are no longer similar to  $\lambda < 0.6$ . Further, for  $\lambda = 0.9$ , the magnitudes of all five frequencies are close; however, the t-test comparison determined that each frequency likely belongs to its own population. For  $\lambda = 0.1$ , the standard deviation of the frequency values is higher than the standard deviations of the same frequencies for the other  $\lambda$ values. More specifically, the standard deviations of frequencies 4 and 5 are higher than those of frequencies 4 and 5 for the other  $\lambda$  values. The magnitude of the frequency values peak near  $\lambda = 0.4$ , afterwards, there is a steady decrease in the values. The magnitudes of the first five frequencies are also higher than the magnitudes of the other polygons, with a maximum near 850Hz.

#### 6.1.2 Pentagon

For the pentagon structures (n=5), the frequency magnitudes form similar pairs to the triangle structures, except the pairings stay consistent up to  $\lambda=0.8$  (Figure 8). Further, for  $\lambda=0.9$  the magnitudes of all the frequencies except frequency 1 are close in magnitude, similar to what was observed with the triangle at  $\lambda=0.7$ . The magnitude of the frequency values peaks near  $\lambda=0.5$ . Overall, standard deviations are small for the pentagon structures. The magnitudes of all the frequency values are smaller than their counterparts (same  $\lambda$  and frequency number) for the triangle structures, appearing to be around half the magnitude in most cases. The maximum frequency value is around 400Hz.

# 6.1.3 Hexagon

The frequency magnitudes for the hexagon structures (n = 6) follow the same pairing as the pentagon but stay consistent longer, including  $\lambda = 0.9$  (Figure 8), which is the highest value of  $\lambda$  that maintains the pairing. The magnitude of the frequency values peaks around  $\lambda = 0.5$ , with a maximum frequency value of around 350Hz. Frequencies 4 and 5 at  $\lambda = 0.1$  and  $\lambda = 0.9$  have a higher standard deviation than the other frequency standard deviations. For 0.2 through 0.8 fractional distance moved along the line ( $\lambda = 0.2 - 0.8$ ), the standard deviations of the magnitudes of the frequencies are smaller in comparison with the previous values. The hexagon structures also tend to have lower frequency magnitudes than their counterparts for the pentagon and triangle; however, there is not as steep of a decrease from pentagon to hexagon as there was from triangle to pentagon.

# 6.1.4 Octagon

The same pairing seen before in the other structures occurs for the octagon structure (n=8) (Figure 8). The pairings stay consistent up to and including 0.9 fractional distance moved along the line  $(\lambda=0.9)$ , just like the hexagon structures. Frequencies 4 and 5 also do not drop in magnitude as much from  $\lambda=0.7$  to  $\lambda=0.9$  as they did for the hexagon structures. The magnitude of the frequency values peak near  $\lambda=0.5$ , similar to the pentagon and hexagon. The octagon structures also tend to have lower frequency magnitudes than their counterparts for the hexagon. For 0.7 through 0.9 fractional distance moved along the line  $(\lambda=0.7-0.9)$ , the magnitudes of frequency 1 are close to each other. This same pattern occurs for frequencies 2 and 3.

Some interesting general results can also be noted. There seems to be a point where the distance along the line starts affecting the frequency values less (Figure 8). For the pentagon, hexagon, and octagon structures where  $\lambda=0.7-0.9$ , the magnitudes for frequency 1 are similar. For the hexagon and octagon structures where  $\lambda=0.7-0.9$ , the magnitudes for frequencies 2-3 are similar. Also, as the number of vertices, n, increases, the pairings stay consistent for higher values of  $\lambda$  (Figure 8). For the triangle, the pairings are only consistent up to  $\lambda=0.5$ , while for the octagon, the pairings are consistent

up to  $\lambda=0.9$ . Further, as the number of vertices, n, increases, the magnitude of the frequency values decreases except for when pairing happens (Figure 8). For example, frequency 1 for  $\lambda=0.1$  for the triangle is higher than frequency 1 for  $\lambda=0.1$  for the pentagon, which is higher than frequency 1 for  $\lambda=0.1$  for the octagon. However for  $\lambda=0.9$ , since the triangle (n=3) does not have pairing at this  $\lambda$ , the magnitudes of frequencies 2 and 3 actually increase for the pentagon (n=5) because pairing occurs.

The results can also be visualized by analyzing the mode shapes and displacement of the structure at the frequencies found (Figure 6). Several interesting results were found. For frequency 1 with all the polygons, the largest displacement occurred in the center of the structure. For frequencies 2 and 3 for all the polygons, there is a hill (positive displacement in z) on one side, while there is a valley (negative displacement in z) on the other side. Frequencies 2 and 3 have similar-looking structural displacements, but the hills and valleys are located in different sections. The displacement of the triangle structure for frequency 4 does not look like the displacement of the pentagon and octagon structures for frequency 4. The triangle structure has three hills located near the vertices and one valley located in the center of the structure. The pentagon and hexagon structures have two hills and two valleys and appear similar to each other.

### **6.2** Tensile Testing

We also conducted a tensile testing experiment on four wallpaper symmetry patterns. A two-way ANOVA for thirty samples at various and T showed that the null hypothesis can be rejected, meaning that there are significant differences between the mean values for both  $\lambda$  and the number of points T. The test also showed that the interaction between the two variables is significant. In general, the porosity values were within 0.1 when compared across the same number of points and the same symmetry and across the same  $\lambda$ . There were only a few exceptions with the p6 symmetry, which had different porosity values, which can be observed in the appendix (Table 2).

Some interesting general observations were found. In general, as the number of points increases for a given  $\lambda$ , the average stress also increases (Figure 12). Also for the p2, p3, and p4 symmetries, this increase appears to be greater when  $\lambda=0.4$  or  $\lambda=0.6$  than when  $\lambda=0.2$  or  $\lambda=0.8$ . For the p6 wallpaper symmetry, when  $\lambda=0.6$ , the overall average stress increases less as the number of points increases.

In general, each symmetry tended to have a  $\lambda$  at which the maximum average stress occurred (Figure 12).

This maximum point seems to occur at  $\lambda=0.4$  for p6 symmetries and the p2 symmetry at 300 points, at  $\lambda=0.6$  for the p2, p3, and p4 symmetries, and at  $\lambda=0.8$  for the p6 symmetry at 100 points.

# 6.2.1 *p2 Symmetry*

The maximum for the p2 wallpaper symmetry occurs near  $\lambda=0.5$  for all values of T (Figure 12 and 9). Across all the values of T, the magnitudes of average Von Mises stress values for  $\lambda=0.4$  and  $\lambda=0.6$  are similar. Further, the distribution of the average stress appears to be parabolic as the fractional distance along the line,  $\lambda$ , increases.  $\lambda=0.2$  has the lowest average stress, increasing when  $\lambda=0.4$ . It stays about the same when  $\lambda=0.6$  and then decreases when  $\lambda=0.8$ . As the number of points increases, the average stress also increases. For example, when  $\lambda=0.2$  and n=100, the average stress is lower than when n=200, which are both lower than n=300.

# 6.2.2 *p3 Symmetry*

For the p3 wallpaper symmetry, the maximum values for the wallpaper symmetries appear to occur around  $\lambda=0.6$  for all the number of points generated (Figure 12 and 10). The average stress values start at the lowest value when  $\lambda=0.2$  and increases as  $\lambda$  increases. The stress value when  $\lambda=0.8$  is lower than when  $\lambda=0.6$  for all of the values T. When  $\lambda=0.2$  and  $\lambda=0.8$ , the increase in the average stress as T increases is less than when  $\lambda=0.4$  and  $\lambda=0.6$ . The mean of the average stress for  $\lambda=0.2$  only increases by about 0.75 MPa, but increases by about 3 MPa for  $\lambda=0.4$ . Further, it increases by about 3 MPa for  $\lambda=0.6$  and only 0.5 MPa for  $\lambda=0.8$ . Finally, as the number of points generated(T) increases, the average stress also increases, which is a similar result to the p2 wallpaper symmetry.

#### *6.2.3 p4 Symmetry*

For the p4 wallpaper symmetry, the distribution of the average stress as  $\lambda$  increases is similar to the distribution for the p3 wallpaper symmetry. When  $\lambda=0.2$ , the average stress is at its lowest value for all the values of T (Figure 12 and 9). The average stress increases as  $\lambda$  increases from 0.2 to 0.4 to 0.6. When  $\lambda=0.6$ , the average stress value appears to reach a maximum value. The trend is the same for all values of T tested. Similar to both the p2 and p3 wallpaper symmetries, the average stress increases for a given  $\lambda$  as the number of points increases. Similar to the p3 wallpaper symmetry, the difference of the average stress values across varying T is larger when  $\lambda=0.4$  and  $\lambda=0.6$  than  $\lambda=0.2$  and  $\lambda=0.8$ . The av-

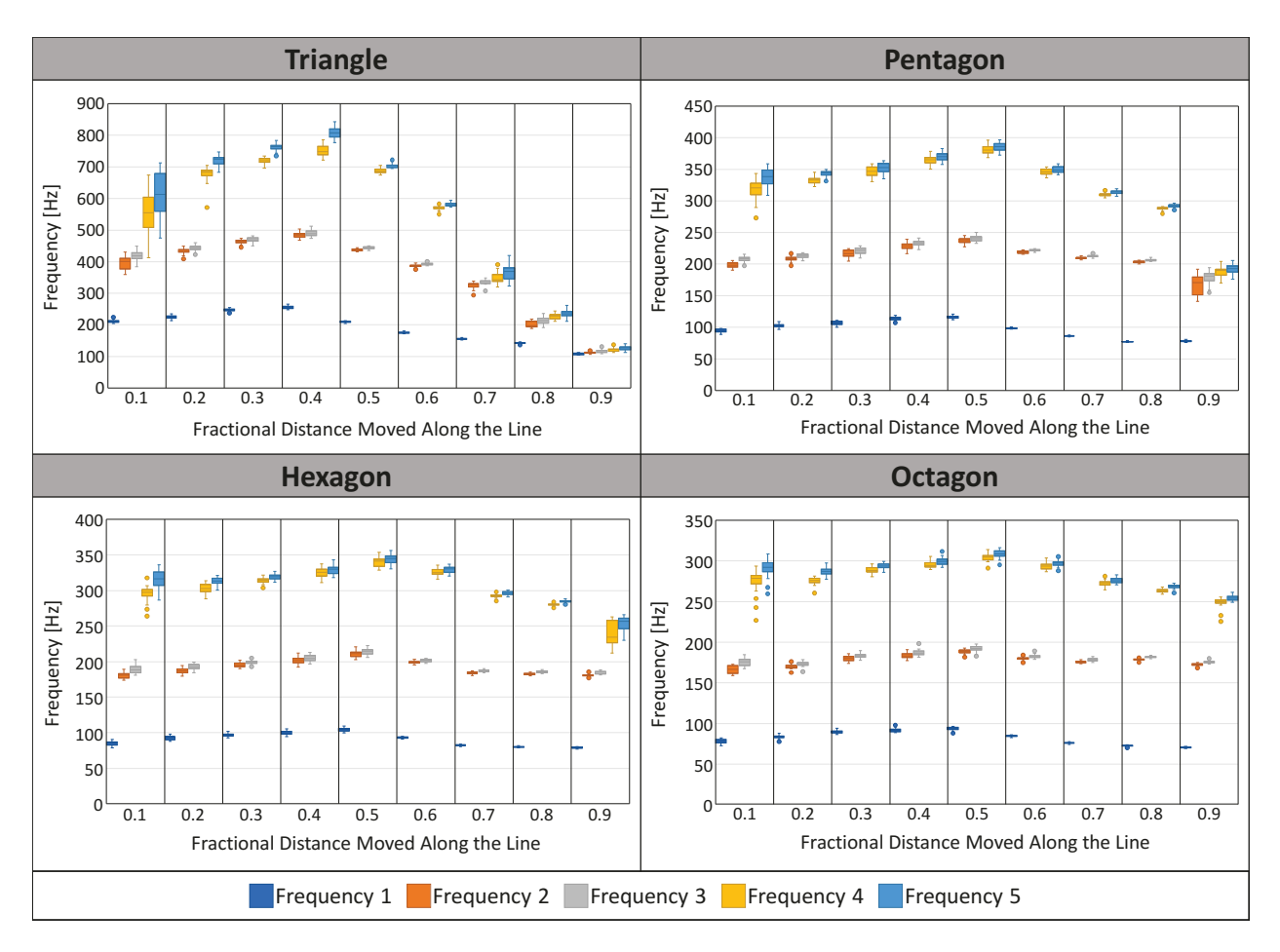


Fig. 8. The first five frequencies found for the structures generated with the fractional distance moved,  $\lambda$  varying from 0.1-0.9 by an interval of 0.1. Each set of parameters was run 25 times and the box plots for each frequency number at each distance are shown.

erage stress only increases by about 1 MPa when  $\lambda=0.2$  and 0.8 MPa when  $\lambda=0.8$ , but increases by 3 MPa when  $\lambda=0.4$  and 2 MPa when  $\lambda=0.6$ .

# 6.2.4 p6 Symmetry

For the p6 wallpaper symmetry, unlike the p2, p3, and p4 symmetries, the  $\lambda$  at which the maximum average stress occurs changes depending on T. For T=100, the maximum occurs when  $\lambda=0.8$  (Figure 12 and 10). For both T=200,300, the maximum average stress occurs when  $\lambda=0.4$ . Further, for T=300, the average stress at  $\lambda=0.4$  is larger than the average stress when  $\lambda=0.8$  by a larger amount than T=200. The difference between the average stress for T=300 when  $\lambda=0.4$  and  $\lambda=0.8$  is near 3.5 MPa, but is only around 1 MPa for T=200. There is also very little change between the average stress values when  $\lambda=0.8$  as T increases. There is a similar occurrence when  $\lambda=0.6$ , but the change is

slightly larger. However, when  $\lambda = 0.2$  and  $\lambda = 0.4$ , the average stress increases as the number of points increases, similar to the p2, p3, and p4 wallpaper symmetries.

# 7 DISCUSSION

# 7.1 Connecting Mechanics to Geometry

# 7.1.1 Modal Testing

We observe a strong connection between mechanical properties and the chaos game parameters. For example, an increase in the number of vertices of the polygon generally decreases the magnitude of the modal frequencies. We also observe a non-linear relationship between  $\lambda$  and frequency which was not expected since  $\lambda$  only changes the distance along a line. This was most notable in the triangle and pentagon case where  $\lambda=0.9$  results in a similar behavior for all frequency values. These overarching observations strongly indicate a fundamental connection between the geometric parameters and mechani-

	Distanc	ce = 0.2	Distanc	ce = 0.4	Distanc	ce = 0.6	Distance = 0.8	
	undeformed deformed		undeformed deformed		undeformed deformed		undeformed	deformed
P4 Symmetry								38 全 38 年
P2 Symmetry								

Fig. 9. An example of several structures with P4 and P2 symmetries and their resulting deformation after tensile loading.

	Distanc	ce = 0.2	Distanc	ce = 0.4	Distanc	ce = 0.6	Distance = 0.8		
	undeformed	deformed	undeformed	eformed deformed		deformed	undeformed	deformed	
P6 Symmetry	*	****** ****** *****	•						
P3 Symmetry				A SA		数			

Fig. 10. An example of several structures with P6 and P3 symmetries and their resulting deformation after tensile loading.

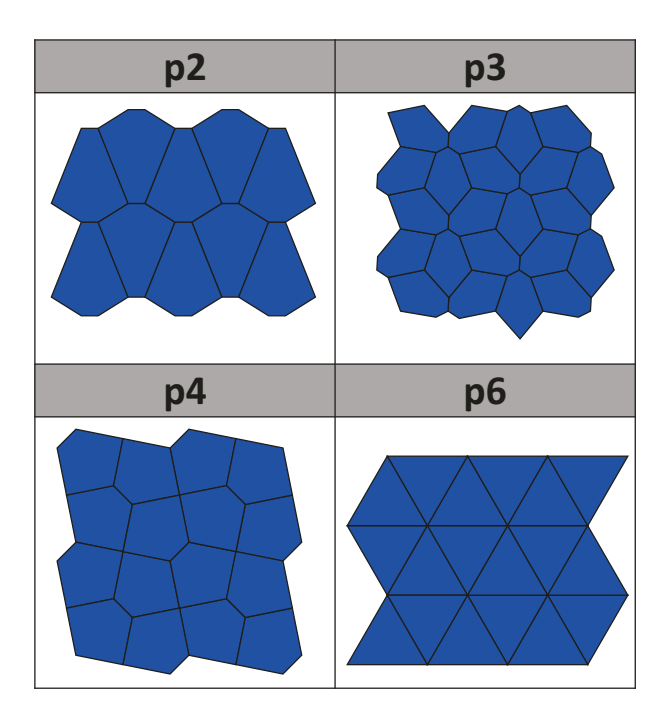


Fig. 11. The polygons that are created from the wallpaper symmetries used in this work are shown with p2, p3, p4, and p6

cal response, at least for natural frequencies.

# 7.1.2 Tensile Testing

Similar to the modal testing, there is a strong connection between the mechanical properties and the chaos parameters. In this case, the number of edges and their locations were controlled by the starting wallpaper symmetry, while the number of points and  $\lambda$  are input parameters.

We can draw several interesting observations and conclusions from the results. A large number of chaos sites can be visualized at the maximum average stress observed in the results (Figure 13). This shows at  $\lambda=0.5$  for p2, which is where the maximum average stress occurs. The structure does not appear to be a fractal by looking at the sites. This is because the  $\lambda$  value is too large for the small edges of the polygon. However, for p3 at  $\lambda=0.6$ , the shape appears to be a fractal and has some self-similarity, but near the short edges, it appears to be just a cluster of points. For the p4 pattern,  $\lambda=.6$  the points look like a fractal structure and are similar to a Sierpinski pentagon, with the only difference being that the p4 pentagon is not a regular pentagon. A very interesting observation is that for the p6 pattern (which produced an equilateral triangle)

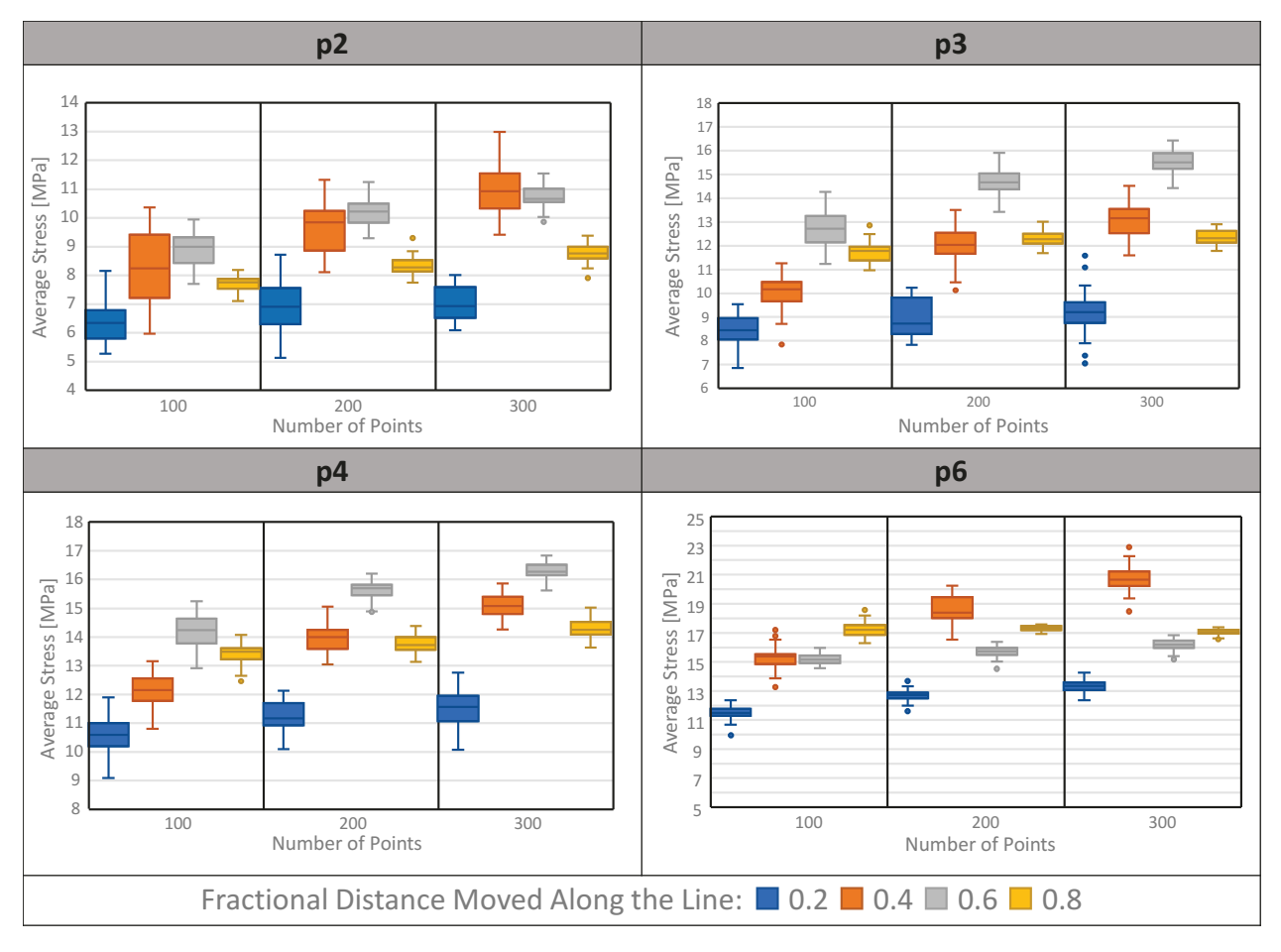


Fig. 12. The average stress for all the tensile tested parts is shown separated by the symmetry type, number of points (T), and  $\lambda$ . Each parameter set was run 30 times, and the box plots are shown with any outliers also represented by points.

the maximum average stress fluctuates between  $\lambda=.4$  and  $\lambda=.6$  depending on the number of points. When  $\lambda=.5$ , the structure is the Sierpinski triangle, and the other lambda values also exhibit points that can be easily recognized as a fractal set of points. All symmetries other than p6 are not regular polygons, with the p4 polygon being close to a regular pentagon.

Another interesting link between  $\lambda$  and the average stress is that all of the structures have the minimum average stress at  $\lambda=0.2$ . At this value of  $\lambda$ , the chaos sites have very little resemblance to a fractal structure and are seemingly random. This is an interesting observation as the structures are similar to stochastic structures.

Because of this, we believe that there is a fundamental link between the degree to which a polygon is a regular polygon and the  $\lambda$  at which the maximum average stress occurs.

# 7.2 Behavioral Patterns

#### 7.2.1 Modal Testing

One behavioral pattern we observe is that a value of  $\lambda$  at which the frequencies appear to reach a maximum value. This is related to how sensitive a given polygon (n) is to the  $\lambda$  value. For example, while  $\lambda=0.5, n=3$  results in a Sierpiński triangle,  $\lambda=0.5, n=8$  (i.e. octagon) has no discernible fractal (Figure 4). Furthermore, for the triangle there is a decrease in modal frequencies only near  $\lambda=0.5$  (i.e. the Sierpiński triangle case). For an octagon and triangle at  $\lambda=0.75$  there is a clear fractal structure appearing which may relate to the decrease in the modal frequencies observed in octagon before  $\lambda=0.75$ . In another example, we find that for n=5 (i.e. a pentagon), the Sierpiński-type fractal occurs only at  $\lambda=\frac{2}{3}$ . This could be a reason why there is a decrease in the modal frequencies near  $\lambda=\frac{2}{3}$  for the pentagon.

Another behavioral pattern that we observed occurred in nearly all of the structures was that of the pairing

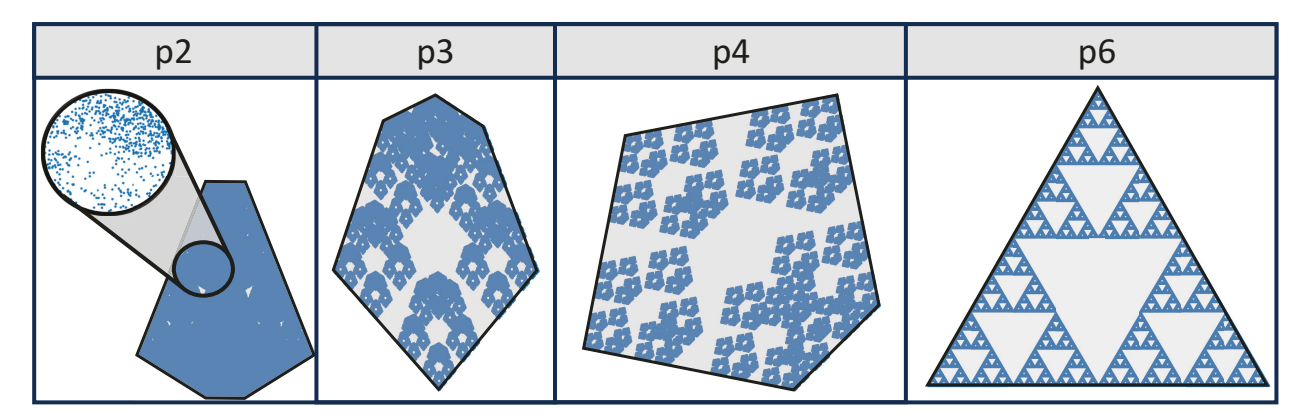


Fig. 13. The fractal pattern at the maximum value for each wallpaper symmetry are shown, specifically p2 at  $\lambda=0.5$ , p3 at  $\lambda=0.6$ , p4 at  $\lambda=0.6$ , and p6 at  $\lambda=0.5$ .

of the results. This can first be observed in our first experiment wherein the second and third natural frequencies have close mean values while the fourth, fifth, and sixth frequencies form another cluster of close mean values (Table 1). Similarly, we observed the clustering of mean values for several other cases as well (Figure 8). The only structures where this pairing did not occur was for high values of  $\lambda$  in the triangle and pentagon in order to validate that each member of a pairing originated from a separate population, a t-value comparison was conducted. In every case, the p < 0.05 means that there is reason to believe that members of a pairing originate from different populations. The largest p-values that we found in our selective t-tests was p = 0.04 for  $(n = 6, \lambda = 0.5)$  between fourth and fifth natural frequencies. Similarly, we get p = .03 for  $(n = 3, \lambda = 0.9)$  and  $(n = 5, \lambda = 0.9)$ between fourth and fifth frequencies. Even here, note that the p-value is safely below the threshold of p < .05. While we cannot posit the reason for these relatively close distributions, we do observe visual similarity in terms of the deformation across the first few modes. For example, the second and third natural frequencies generally display high qualitative similarity for each polygonal domain (Figure 6).

# 7.2.2 Tensile Testing

From the results, all tests have several commonalities. The first behavioral pattern we observe is that the minimum average stress for every set occurs when  $\lambda=0.2$ . All the wallpaper symmetries have an increase in the average stress when  $\lambda$  increases to 0.4 from 0.2, but as  $\lambda$  increases more, the different wallpaper symmetries behave differently.

Another behavioral pattern that is observed is that the maximum average stress happens when  $0.4 \le \lambda \le 0.6$ 

in all but one of the test cases. For the p2 wallpaper symmetry, the maximum average stress occurs near  $\lambda = 0.5$ . For the p3 and p4 wallpaper symmetries, the maximum average stress occurs near  $\lambda = 0.6$ . For the p6 wallpaper symmetry, the maximum average stress occurs at  $\lambda = 0.8$ for T=100 and then  $\lambda=0.4$  for T=200 and T=300. This could be because the points become less clustered as  $\lambda$  increases (Figure 13). When  $\lambda$  is closer to 0, the points do not move much at each iteration and therefore do not cluster much (Figure 4). When  $\lambda$  is closer to 1, the points are clustered near the vertices of the polygon. This clustering could create a region that is more resistant to stress, which could increase the maximum average stress. This could be a potential reason why the maximum average stress occurs when  $0.4 \le \lambda \le 0.6$  for all but one of the test cases.

Another similarity between the tests is that as lambda increases, there is a near-parabolic curve for the average stress in each symmetry except for p6. Meaning that there is an increase in average stress up to the maximum and then a decrease in average stress. The reason that this pattern may not exist in p6 could be due to the fact that it is a regular triangle, and this causes p6 not to follow the same pattern. This difference could also be due to the fact of having non-similar porosity values. The final behavioral pattern that is observed is that the p3 and p6 symmetries have a larger spread of values for the average stress than the p2 and p4 symmetries. The p2 and p4 symmetries only have a spread of around 6 MPa and 7 MPa, respectively. However, the p3 and p6 symmetries have a spread of around 8 MPa and 10 MPa, respectively.

### 7.3 Limitations and Future work

There are several questions that require further exploration in this work. First, there are several variations to

the chaos game with extended rules for point generation. One example is applying a preference model during the random selection of polygonal vertices that leads to new types of structures emerging. For example, a rule could be that a vertex cannot be chosen twice in a row. Given that this is a rich design space, further expansive investigation is needed to explore this aspect further. Secondly, while we have shown chaos sites for non-regular identical polygons, a wide range of other non-regular non-identical polygons can be explored and create different properties. Adding to this, an obvious extension would be to consider arbitrary 2D domains wherein we can apply our method to triangulated domains. Thirdly, it is important to evaluate our current structures for different multi-physical responses. Another intriguing future direction is to extend the idea to 3D structures. Interestingly, this can be easily done since the chaos game works even for selective 3D polyhedral domains. As a result, it would be interesting to explore sponge-type as well as frame-type structures in 3D domains based on using the edges and faces of 3D Voronoi cells. Overall, we see an immense potential for self-similar structures in generative design.

#### 8 CONCLUSION

In this paper, we introduced a forward-design approach for generative statistically self-similar structures based on fractal geometry. Using a combination of chaos game and Voronoi tessellation, we show that it is possible to generate families of structures whose geometric similarities carry forward in terms of mechanical response. Using our method, we demonstrated this within the concrete context of natural modes and tensile testing of the structures generated. Our experiments conclusively show that the parameters of the chaos game offer a controlled way to tune the mechanical response and enable the generation of populations of shapes rather than a single optimal shape. We further demonstrated tractable relationships across different parameters (especially fractional distance) of the chaos game. This is an essential requirement for a generative design workflow. We believe that this work is merely a starting point for a potentially rich research direction in the domain of generative structural design.

# A APPENDIX

We have included the average porosity values and the stand deviation for the structures generated and tensile tested.

# **ACKNOWLEDGEMENTS**

This work was supported by the National Science Foundation (NSF) Awards #2048182 (Engineering Design and Systems Engineering Program). Any opinions, findings, and conclusions or recommendations expressed in this material are those of the authors and do not necessarily reflect the views of the NSF.

# REFERENCES

- [1] Shea, K., Aish, R., and Gourtovaia, M., 2005, "Towards integrated performance-driven generative design tools," *Automation in Construction*, **14**(2), pp. 253–264.
- [2] Buonamici, F., Carfagni, M., Furferi, R., Volpe, Y., and Governi, L., 2020, "Generative design: an explorative study," *Computer-Aided Design and Applications*, **18**(1), pp. 144–155.
- [3] Oh, S., Jung, Y., Kim, S., Lee, I., and Kang, N., 2019, "Deep generative design: Integration of topology optimization and generative models," *Journal of Mechanical Design*, **141**(11).
- [4] Al-Jawfi, R. A., Al-Helali, B. M., and Ahmed, A. M., 2014, "Fractal image compression using selforganizing mapping," *Applied Mathematics*, 5(12), pp. 1810–1819.
- [5] Rian, I. M., and Sassone, M., 2014, "Fractal-based generative design of structural trusses using iterated function system," *International journal of space structures*, **29**(4), pp. 181–203.
- [6] Fan, J. A., Yeo, W.-H., Su, Y., Hattori, Y., Lee, W., Jung, S.-Y., Zhang, Y., Liu, Z., Cheng, H., Falgout, L., et al., 2014, "Fractal design concepts for stretchable electronics," *Nature communications*, 5(1), p. 3266.
- [7] Mishra, J., and Mishra, S., 2007, *L-system Fractals* Elsevier.
- [8] Barnsley, M. F., and Demko, S., 1985, "Iterated function systems and the global construction of fractals," *Proceedings of the Royal Society of London.* A. Mathematical and Physical Sciences, 399(1817), pp. 243–275.
- [9] Schroeder, M., 2009, Fractals, chaos, power laws: Minutes from an infinite paradise Courier Corporation.
- [10] Deschavanne, P. J., Giron, A., Vilain, J., Fagot, G., and Fertil, B., 1999, "Genomic signature: characterization and classification of species assessed by chaos game representation of sequences.," *Molecular biology and evolution*, 16(10), pp. 1391–1399.
- [11] Jampour, M., Yaghoobi, M., Ashourzadeh, M., and Solemani, A., 2010, "A new fast technique for fin-

	Number of Points	Fractional Distance Moved Along the Line								
Symmetry		0.2		0.4		0.6		0.8		
		Mean	StdDev	Mean	StdDev	Mean	StdDev	Mean	StdDev	
p2	100	0.913	0.008	0.887	0.016	0.871	0.008	0.881	0.005	
p2	200	0.896	0.005	0.848	0.017	0.851	0.009	0.863	0.004	
	300	0.882	0.009	0.837	0.017	0.834	0.009	0.851	0.006	
р3	100	0.874	0.010	0.851	0.015	0.795	0.017	0.823	0.007	
p5	200	0.850	0.009	0.810	0.016	0.747	0.016	0.799	0.004	
	300	0.833	0.009	0.788	0.012	0.714	0.011	0.783	0.003	
p4	100	0.850	0.007	0.817	0.011	0.767	0.016	0.808	0.009	
p <del>4</del>	200	0.820	0.007	0.775	0.014	0.718	0.009	0.783	0.004	
	300	0.808	0.009	0.746	0.011	0.698	0.008	0.763	0.005	
p6	100	0.820	0.009	0.732	0.018	0.731	0.008	0.746	0.009	
	200	0.781	0.008	0.645	0.035	0.673	0.008	0.688	0.004	
	300	0.757	0.008	0.574	0.027	0.632	0.009	0.662	0.005	

Table 2. Mean and Standard Deviation of the Porosity of 30 Test Samples for Each Set of Parameters. The porosity is the measure of void or empty space within each structure.

- gerprint identification with fractal and chaos game theory," Fractals-complex Geometry Patterns and Scaling in Nature and Society FRACTALS, 18, 09.
- [12] Biswas, B., Ghatak, R., and Poddar, D. R., 2017, "A fern fractal leaf inspired wideband antipodal vivaldi antenna for microwave imaging system," *IEEE Transactions on Antennas and Propagation*, **65**(11), pp. 6126–6129.
- [13] Prusinkiewicz, P., 1986, "Graphical applications of l-systems," In Proceedings of graphics interface, Vol. 86, pp. 247–253.
- [14] Rosen, D. W., 2007, "Computer-aided design for additive manufacturing of cellular structures," *Computer-Aided Design and Applications*, **4**(5), pp. 585–594.
- [15] Ren, X., Das, R., Tran, P., Ngo, T. D., and Xie, Y. M., 2018, "Auxetic metamaterials and structures: a review," *Smart materials and structures*, **27**(2), p. 023001.
- [16] Wang, H., Chen, Y., and Rosen, D. W., 2005, "A hybrid geometric modeling method for large scale conformal cellular structures," In ASME 2005 International Design Engineering Technical Conferences and Computers and Information in Engineering Conference, American Society of Mechanical

- Engineers Digital Collection, pp. 421–427.
- [17] Wang, H., Zhang, Y., Lin, W., and Qin, Q.-H., 2020, "A novel two-dimensional mechanical metamaterial with negative poisson's ratio," *Computational Materials Science*, **171**, p. 109232.
- [18] Ai, L., and Gao, X.-L., 2017, "Metamaterials with negative poisson's ratio and non-positive thermal expansion," *Composite Structures*, **162**, pp. 70–84.
- [19] Eschenauer, H. A., and Olhoff, N., 2001, "Topology optimization of continuum structures: a review," *Appl. Mech. Rev.*, **54**(4), pp. 331–390.
- [20] Sigmund, O., and Maute, K., 2013, "Topology optimization approaches: A comparative review," *Structural and Multidisciplinary Optimization*, 48(6), pp. 1031–1055.
- [21] Bielefeldt, B. R., Akleman, E., Reich, G. W., Beran, P. S., and Hartl, D. J., 2019, "L-systemgenerated mechanism topology optimization using graph-based interpretation," *Journal of Mechanisms and Robotics*, **11**(2).
- [22] Ward, R. M., Bielefeldt, B. R., and Hartl, D. J., 2020, "Design of tailorable stiffness structures using 1-system topology optimization," In Behavior and Mechanics of Multifunctional Materials IX, Vol. 11377, SPIE, pp. 112–122.

- [23] Tian, J., Tang, K., Chen, X., and Wang, X., 2022, "Machine learning-based prediction and inverse design of 2d metamaterial structures with tunable deformation-dependent poisson's ratio," *Nanoscale*.
- [24] White, D. A., Arrighi, W. J., Kudo, J., and Watts, S. E., 2019, "Multiscale topology optimization using neural network surrogate models," *Computer Methods in Applied Mechanics and Engineering*, **346**, pp. 1118–1135.
- [25] Garland, A. P., White, B. C., Jensen, S. C., and Boyce, B. L., 2021, "Pragmatic generative optimization of novel structural lattice metamaterials with machine learning," *Materials Design*, **203**, p. 109632.
- [26] Podroužek, J., Marcon, M., Ninčević, K., and Wan-Wendner, R., 2019, "Bio-inspired 3d infill patterns for additive manufacturing and structural applications," *Materials*, **12**(3).
- [27] Ebert, M., Subramanian, S. G., Akleman, E., and Krishnamurthy, V. R., 2020, "Generative infills for additive manufacturing using space-filling polygonal tiles," In International Design Engineering Technical Conferences and Computers and Information in Engineering Conference, Vol. 84010, American Society of Mechanical Engineers, p. V11BT11A014.
- [28] Icking, C., Klein, R., Ma, L., Nickel, S., and Weißler, A., 2001, "On bisectors for different distance functions," *Discrete applied mathematics*, **109**(1-2), pp. 139–161.
- [29] Howison, M., and Séquin, C. H., 2009, "Cad tools for creating space-filing 3d escher tiles," *Computer-Aided Design and Applications*, **6**(6), pp. 737–748.
- [30] Subramanian, S. G., Eng, M., Krishnamurthy, V. R., and Akleman, E., 2019, "Delaunay lofts: A biologically inspired approach for modeling space filling modular structures," *Computers & Graphics*, **82**, pp. 73–83.
- [31] Schumacher, C., Marschner, S., Gross, M., and Thomaszewski, B., 2018, "Mechanical characterization of structured sheet materials," *ACM Transactions on Graphics (TOG)*, **37**(4), pp. 1–15.
- [32] Martínez, J., Skouras, M., Schumacher, C., Hornus, S., Lefebvre, S., and Thomaszewski, B., 2019, "Star-shaped metrics for mechanical metamaterial design," *ACM Transactions on Graphics (TOG)*, **38**(4), pp. 1–13.
- [33] Sun, F., Lai, C., and Fan, H., 2016, "In-plane compression behavior and energy absorption of hierarchical triangular lattice structures," *Materials & Design*, **100**, pp. 280–290.
- [34] Zhikharev, L., 2021, "A sierpiński triangle geomet-

- ric algorithm for generating stronger structures," In Journal of Physics: Conference Series, Vol. 1901, IOP Publishing, p. 012066.
- [35] Cheng, Q., Yin, J., Wen, J., and Yu, D., 2023, "Mechanical properties of 3d-printed hierarchical structures based on sierpinski triangles," *International Journal of Mechanical Sciences*, **247**, p. 108172.
- [36] Liang, H., Hao, W., Xue, G., Liu, B., Pu, Y., and Ma, F., 2022, "Parametric design strategy of a novel self-similar hierarchical honeycomb for multi-stage energy absorption demand," *International Journal of Mechanical Sciences*, **217**, p. 107029.
- [37] Tao, Y., Li, W., Wei, K., Duan, S., Wen, W., Chen, L., Pei, Y., and Fang, D., 2019, "Mechanical properties and energy absorption of 3d printed square hierarchical honeycombs under in-plane axial compression," *Composites Part B: Engineering*, **176**, p. 107219.
- [38] Chen, Y., Li, T., Jia, Z., Scarpa, F., Yao, C.-W., and Wang, L., 2018, "3d printed hierarchical honeycombs with shape integrity under large compressive deformations," *Materials Design*, **137**, pp. 226–234.
- [39] Jeffrey, H., 1992, "Chaos game visualization of sequences," *Computers Graphics*, **16**(1), pp. 25–33.
- [40] Talatahari, S., and Azizi, M., 2020, "Optimization of constrained mathematical and engineering design problems using chaos game optimization," *Computers Industrial Engineering*, **145**, p. 106560.
- [41] Ramadan, A., Kamel, S., Hussein, M. M., and Hassan, M. H., 2021, "A new application of chaos game optimization algorithm for parameters extraction of three diode photovoltaic model," *IEEE Access*, **9**, pp. 51582–51594.
- [42] Barnsley, M. F., 2014, *Fractals everywhere* Academic press.
- [43] Ewins, D. J., 2009, *Modal testing: theory, practice and application* John Wiley & Sons.
- [44] Avitabile, P., 2001, "Experimental modal analysis," *Sound and vibration*, **35**(1), pp. 20–31.